Morphological Characteristics of Liesegang Rings and Their Simulations

Hans-Jürgen Krug* and Hermann Brandtstädter

Technische Universität Berlin, Institut für Theoretische Physik, AG Dissipative Strukturen, Sekr. PN 7−1, Hardenbergstrasse 36, D-10623 Berlin, Germany

Received: March 30, 1999; In Final Form: July 23, 1999

Numerical simulations of Liesegang systems are performed both with a prenucleation and a postnucleation model. Special interest is dedicated to two-dimensional morphological peculiarities of ring systems. With the prenucleation model, apparent bifurcations or branch points (anastomoses) can be created by adjacent trains of bands having different interband spaces or band positions shifted to each other. Spiral systems arise when the circular symmetry of concentric Liesegang rings is broken by at least one branch point. The postnucleation model comprises both formation of colloidal particles which form a turbidity zone and transition of these nuclei to solid particles which undergo Ostwald ripening at the expense of the colloids. The model demonstrates how Liesegang bands of solid particles arise from a primary turbidity zone which surrounds the expanding ring system. Because of rapid competitive particle growth, rings or bands may no longer grow continuously in transversal directions. They become arranged in chains of single filaments or spots forming a transversal rhythm. Finally, longitudinal alleys of gaps appear in continuous trains of Liesegang bands.

1. Introduction

An early report on periodic precipitation, with calcium oxalate, was given by W. M. Ord in 1879.[1] Systematic investigation of this phenomenon was initiated by the experiments of photochemist R. Ed. Liesegang in 1896.[2] His classical experiment on a glass plate consisted of radial diffusion of silver nitrate in a photogelatin layer with potassium dichromate. Both visual attraction of the periodic precipitation and the apparent similarity to geological textures[3−5] and patterns in plant and animal biology[6,7] continue to stimulate research.[8−12]

Periodic precipitation has raised from a curiosity to a general phenomenon in colloid chemistry: First, it does not depend on special choice of diffusion media. Besides gelatin or other gels, granular or porous media like quartz sand, sulfur powder, kieselguhr, and gypsum may serve as diffusion matrices.[9,10,13] Periodic precipitation was also observed in gas phase[14,15] and in pure water.[16] Further, beside silver chromate there was found a broad series of hardly soluble salts, pure metals such as gold and mercury, and even organic compounds forming periodic precipitates.[9,10,13] Finally, the phenomenon occurs independently if the precipitating matter is formed in situ by chemical reaction or if the precipitation takes place in evaporating solutions[7] or slowly cooling melts.[17]

Because of the complexity of the Liesegang mechanism arising from the interaction of involved processes, it is only partly understood. The following processes should be taken into account: (1) Chemical reaction and electrolytic dissociation. (2) Concentration dependency of diffusion. (3) Formation of colloid particles prior to precipitation. (4) Coagulation of colloid particles or accumulation of ions. (5) Transition from colloid to crystal phase with increasing supersaturation. (6) Competitive particle growth (Ostwald ripening).

Considering aspects of these processes, different types of models were proposed to describe the phenomenon of periodic banding, as such, and the spacing laws and morphological characteristics of bands. The first model was introduced by Wilhelm Ostwald in 1897 and based on supersaturation of silver chromate. His cycle of supersaturation, precipitation, and depletion still delivers the core of each recent prenucleation model.[18] The supersaturation theory was modeled by Prager,[19] Henisch,[10−11] Dee,[20] and Le Van and Ross,[21] the latter[20,21] emphasizing the necessity of a steep dependence of the nucleation rate on supersaturation.

Band-forming coagulation of colloid particles was proposed by Dhar and Chatterji.[22] The coagulation theory was treated later by Flicker and Ross[16] and Büki et al.[23] Flicker also showed that band formation may take place in gradient-free systems on the basis of autocatalytic coagulation and growth of colloid particles. The recursive influence of electrolyte production on precipitation was considered by Wolfgang Ostwald in his "Diffusion Wave Theory".[24] The role of fluctuations in the nucleation process in periodic precipitation can be considered by cellular automata.[25]

On the basis of experimental observations,[26−28] Ortoleva et al. proposed that sole competition of growing particles can produce bands, even in absence of strong external gradients.[29−31,33] The competitive particle growth (CPG) model represented an application of the Lifshitz−Slyozov instability[32] of competing particle ensembles. Also, morphological characteristics of bands, such as the formation of precipitate-free alleys, single filaments, or spots, can be described by employing postnucleation models.[33−37]

With respect to morphological defects of bands, Liesegang first pointed out that the sharp localization of precipitation bands were due to strong attraction of precipitate to solute material.[38] Precipitation filaments once formed are thus hindered not only in radial but also in transversal growth. Apparent ring defects such as radial alleys of gaps or precipitation filaments located only at the surface of the gelatin layer or onto the glass plate were also caused by rapid local depletion of solute material. Liesegang also described ripening effects in silver halide emulsions and coined the term "Ostwald ripening".[39]

* E-mail: krug@physik.tu-berlin.de

10.1021/jp991092l CCC: $18.00
Published on Web 09/11/1999

Morphological defects were compiled by Küster[40] from the viewpoint of plant biology. He generated arrays of precipitation spots arranged in both radial and transversal rhythms by polycentric diffusion. Diffusion sources with uneven shapes may deliver autonomous ring systems with different spacing sequences which are linked together by branch points or bridges. In some cases, bridges do not appear and leave blank alleys between adjacent ring systems. Liesegang applied the term "anastomoses"[4,41,42] for such branched bands, a term originally coined in medicine. Liesegang first recognized the analogy of branched precipitation patterns to "pseudoclases" of banded minerals.[42] The influence of diffusion source geometry on ring formation was reconsidered later,[43] also with respect to geoscience.[34,35,37] A further interesting case of ring instability is the formation of tree-like crystal growth within the bands.[44,45]

The development of spirals was frequently reported in the literature.[24,27,41,45−52] The first observation of a two-dimensional spiral was published in 1907[46] but only later indicated by Liesegang.[48] Spirals are the consequence of branch points because they break off the concentric symmetry of ideal Liesegang rings. Three-dimensional spirals in cylindrical vessels are generated by apparent initial bifurcations in the sequence of otherwise parallel precipitation disks.[24,27, 45,49−52]

In the present paper, we compare the results of a prenucleation and a postnucleation model by simulations in one and two spatial dimensions. The postnucleation model will consider both colloid formation and competitive particle growth, whereas the prenucleation model involves only the strong nonlinear dependence of nucleation rate on supersaturation. Our special attention is paid to the formation of two-dimensional pattern characteristics as there are branch points, spirals, and single filaments. Our aim is to show how these apparent defects are caused by the mechanisms themselves responding to diffusion source geometry. Finally, we demonstrate by means of the postnucleation model that the appearance of a colloid front prior to nucleation is constitutive for creation of sharp rings.

2. Morphological Characteristics of Liesegang Systems

A typical example of a silver chromate Liesegang ring system with branch points arising from the nonconcentric shape of the diffusion center is given in Figure 1. The ring system decays into several sectors with autonomous spacing sequences. The spatial phase differences arising between adjacent sectors is commonly equalized by apparent branch points or blank spaces arranged radially from the diffusion center. Microscopic inspection of the branch points shows that they consist of three-dimensional bridges, each connecting the lower part of the one band with the upper part of the opposite band and vice versa. Apparent crossing of both bridges is the result of two-dimensional projection only.[40]

A concentric turbidity zone surrounds the whole ring system which serves as the source matter of each freshly arising ring filament. This turbidity zone is most apparent and narrow at early stages of the experiment and becomes pale and broader at later times, as also do the precipitation rings. After creation of the last outer ring, the turbidity is consumed in its vicinity until it vanishes completely between the rings. Such a turbidity zone was first mentioned by Hatschek[53] for the silver chromate system. With respect to the lead iodide system, Le Van and Ross[21] observed a yellow haze, which was interpreted as a colloid phase, before ring formation. Explicit measurements of turbidity zones were performed by Müller et al.[54] for the $Mg(OH)_2$ system and by Lexa and Holba[55] for the silver chromate system. The occurrence of that colloid phase prior to precipitation is considered to be a strong hint in favor of postnucleation theories. Note that the density of the turbidity zone in Figure 1, according to the observations in refs 54 and 55, is nonperiodic, thus, the periodicity of the later solid bands is not preformed by any periodicity of the colloidal zone.

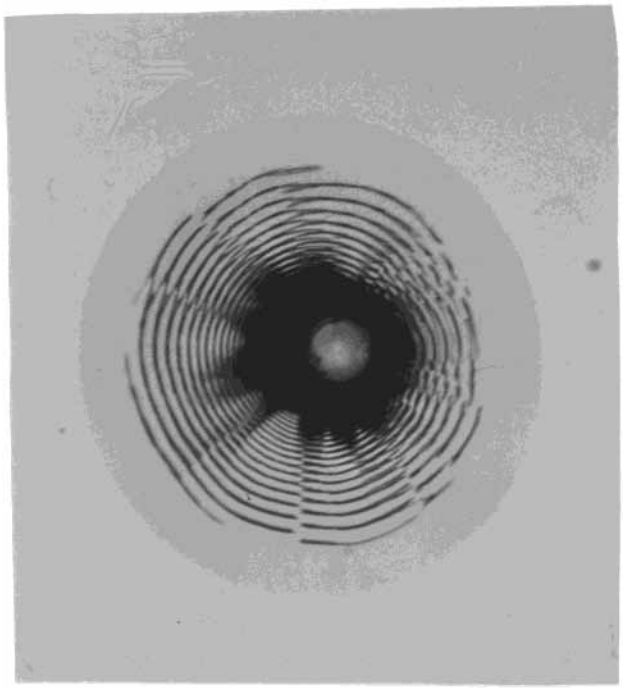

Figure 1. Liesegang rings of silver chromate with apparent bifurcations (branch points, and blank alleys). Photo taken 25 min after start of the experiment. The expanding ring system is enveloped by a moving turbidity zone of colloidal silver chromate. Recipe: 0.5 M $AgNO_3$ solution in the center, 3.4 mM $K_2Cr_2O_7$ in the gelatin. The gelatin layer of 1.0 mm thickness was covered by a plate of plexiglass. The silver nitrate solution (0.3 mL) was applied through a drill hole in the center of the plate. Horizontal field of view: 24 mm.

Inspection of freshly formed rings using the recipe from Figure 1 with in situ X-ray microscopy delivered particle radii between 0.04 and 0.125 μm. Probes taken from the turbidity zone did not contain any particles above the resolution limit (0.01 μm).

Because of the geometry of the diffusion source, the double-centered Liesegang system in Figure 2 exhibits a series of blank radial alleys bordering ring sequences with definite phase shifts to each other. Also, tall stripes of phase-shifted band sequences and single spots are inserted into the background of undisturbed concentric rings.

Figure 3 shows discordances in straight Liesegang bands emanating from an almost even diffusion source. Here, the ring system is divided into stripes with autonomous spacing sequences. Adjacent stripes are separated at first by blank alleys which are superseded by branch point at larger distances from the diffusion source. At other parts, adjacent bands are finally connected by sigmoidal bridges after the decreasing phase difference is sufficiently low.

As mentioned above, spiral systems are created by discordances in concentric ring symmetry. Figure 4 shows a ring system with several anastomoses branching into different directions. A branch point in the upper right part of the system generates a counterclockwise winding spiral which is not canceled out by further bifurcations.

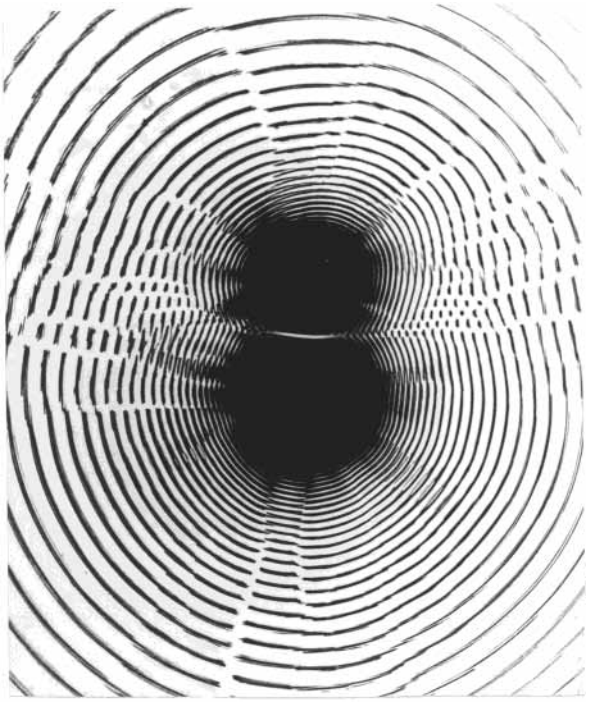

Figure 2. Typical blank alleys and single spots generated by a double-centered Liesegang system (final state). Recipe as in Figure 1. Horizontal field of view: 40 mm.

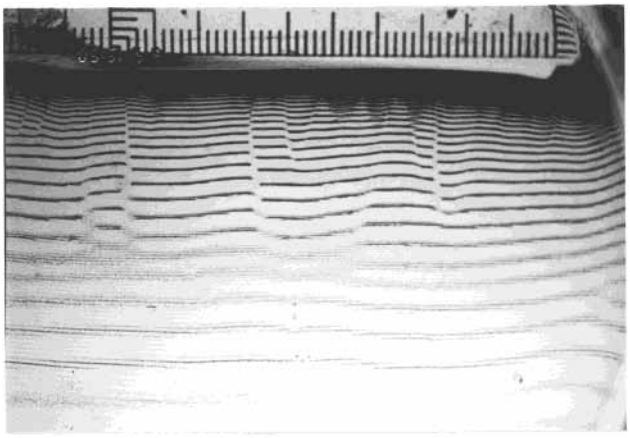

Figure 3. Adjacent areas of Liesegang bands of silver chromate with individual band spacings (final state). Silver nitrate (0.5 M) diffuses from an almost straight line into the gelatin (5.14 mM K_2CrO_4). Areas of bands are either separated by blank alleys or are connected by anastomoses. The secondary rhythm appearing in the lower part is caused by phosphate impurities in the gelatin (see also Figure 4).

3. The Prenucleation Model

First, we want to simulate the appearance of branch points and the phenomenon of spiralization by means of a prenucleation model. The prenucleation model to be employed was originally proposed by Dee.[20] Let us consider now a nonionic chemical reaction of two components resulting in a hardly soluble product. Choosing silver monochromate, we have

$$2AgNO_3 + K_2CrO_4 \rightarrow Ag_2CrO_4 + 2KNO_3 \qquad (R1)$$

In contrast of the experimental observation of a turbidity zone, the Dee model treats the direct conversion of hardly soluble silver salt C (here Ag_2CrO_4) from solution to solid phase via nucleation and linear particle growth. Furthermore, an ionic formulation of reaction R1 is not considered. Despite these

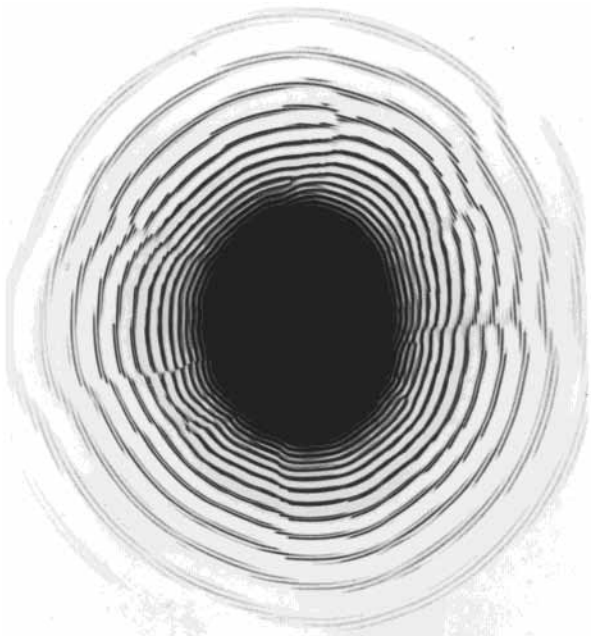

Figure 4. Spiral pattern in a Liesegang system of silver chromate. The spiral branches off from an apparent bifurcation in the upper right part near the diffusion source. Recipe as in Figure 1. Thickness of the gelatin: 1.5 mm. Horizontal field of view: 38 mm.

simplifications, the Dee model generates precipitation patterns because of the strong nonlinearity in the nucleation rate defined as

$$J(s) = J_c s^2 \exp[-(s^*/\ln s)^2] \qquad (1)$$

with $s^* = (4\pi\sigma w^2/3k_BT)^{1/2}$, and $J_c = 4\pi D_C w c_0^2/d$. Here, k_B is the Boltzmann constant, T the temperature, w the capillary length, σ the surface tension of the flat crystal, c_0 the saturation concentration of C (related to big crystals), d twice the molecular diameter, and D_C the diffusion coefficient of C. The supersaturation s is defined as $s = c/c_0$. The nonlinearity in eq 1 is indeed required for delivering periodic precipitation. Accordingly, Venzl and Ross[56] have shown, in a former paper, that a nucleation rate less steep in eq 1 than with $J \sim s^n$ coupled with linear particle growth is not capable to produce patterned precipitation. A steep exponential nucleation rate according to eq 1 was later employed by Le Van and Ross.[21] To enforce precipitation-free interband spaces without Ostwald ripening, they introduced a nucleation rate completely zero below a critical value of supersaturation. Other authors[52,57−59] simply replaced the nucleation term (eq 1) by a Heaviside function in s.

The full system considering chemical reaction, diffusion, and precipitation reads

$$\frac{\partial a}{\partial t} = D_A\Delta a - 2k_{R1}ab$$

$$\frac{\partial b}{\partial t} = D_B\Delta b - k_{R1}ab$$

$$\frac{\partial c}{\partial t} = D_C\Delta c + k_{R1}ab - u(c,t)$$

$$\frac{\partial m}{\partial t} = u(c, t) \qquad (2)$$

where a, b, c, and m are the concentrations of silver nitrate (A), potassium chromate (B), silver chromate (C), and finally the solid phase which is considered to be immobile; k_{R1} is the

reaction velocity constant; D_A, D_B, and D_C are the diffusion coefficients of A, B, and C. The $u(c, t)$ term denotes the loss of c due to precipitation. The concentration of solid phase m is defined as

$$m(x, t) = \frac{4\pi}{3V_m} \int_0^t J(x, t')\, r^3(x, t, t')\, dt' \tag{3}$$

where V_m is the molar volume of the precipitate, r the particle radius, x space, and t time.

Restriction to a linear particle growth according to $dr/dt = g(s - 1)$ permits stepwise differentiation of the integral term in eq 3 and finally numerical integration of system 2. Furthermore, let the initial radius r_0 of a particle created at time t be $r_0 = w \ln s \approx w$. Then we have for $u = dm/dt$

$$u(x, t) = \frac{4\pi}{3V_m}[J(x, t)w^3 + 3g(s - 1) \int_0^t J(x, t')r^2(x, t, t')dt'] \tag{4}$$

Repeated differentiation of the integral term in eq 4 delivers supplemental variables which can be interpreted as averages of radii and surfaces of the particle ensemble at x and t. Let the local average of radii of particles be defined as

$$\langle r(x, t)\rangle = \frac{\int_0^t J(x, t')r(x, t, t')\, dt'}{\int_0^t J(x, t')dt'} \tag{5}$$

with the particle number density p

$$p(x, t) = \int_0^t J(x, t')\, dt' \tag{6}$$

The matter parameters chosen for simulation of the silver chromate system[60] are as follows: $\sigma = 575$ erg cm^{-2}, $c_0 = 9.15 \times 10^{-5}$ mol L^{-1}, $V_m = 60.1$ cm^3 mol^{-1}, $d = 9.2 \times 10^{-8}$ cm (estimated from V_m), $D_A - D_C = 1.0 \times 10^{-5}$ cm^2 s^{-1} (arbitrary), $k_{R1} = 1.0 \times 10^3$ cm^3 mol^{-1} s^{-1} (arbitrary), and $g = 1.0 \times 10^{-7}$ cm s^{-1} (arbitrary).

The capillary length w, calculated from

$$w = \frac{2\sigma V_m}{\upsilon RT} \tag{7}$$

with gas constant R, room temperature T, and the dissociation factor $\upsilon = 3$ for Ag_2CrO_4 attains a numerical value of $w = 9.3 \times 10^{-7}$ cm which is about one degree of order too large to obtain periodic precipitation. Sharply modulated patterns were obtained after decreasing this value to 0.8 to 1.0×10^{-7} cm.[61]

One-Dimensional Simulations. Figure 5 shows a representative plot of a one-dimensional simulation of a Liesegang pattern using the formalism given above. The silver nitrate drop is diffusing there from the left to the right into a medium penetrated with potassium chromate of constant initial concentration b_0. The resulting precipitation pattern $m(x)$ attained an average level of b_0 as it should be. On the other hand, the modulated particle number density $p(x)$ decreases with growing distance from the silver nitrate source whereas the average of the particle radii $\langle r(x)\rangle$ increases. This is in accordance with the common experimental observation that, with increasing distance of bands from the diffusion center, the particle number density decreases accompanied by growing particle radii.

Though the concentration of precipitate m is strongly modulated because of the modulation of p, the spaces between the bands are not completely free of precipitate. This contradicts the experiment which demands clear interband spaces. Void spaces cannot be obtained even with extremely high values of the particle growth rate g, as long as the model is constrained to linear particle growth $dr/dt = g(s - 1)$. Clear interband spaces will be obtained either by vanishing nucleation rates below a critical supersaturation[21] or by postnucleation models to be demonstrated in section 4.

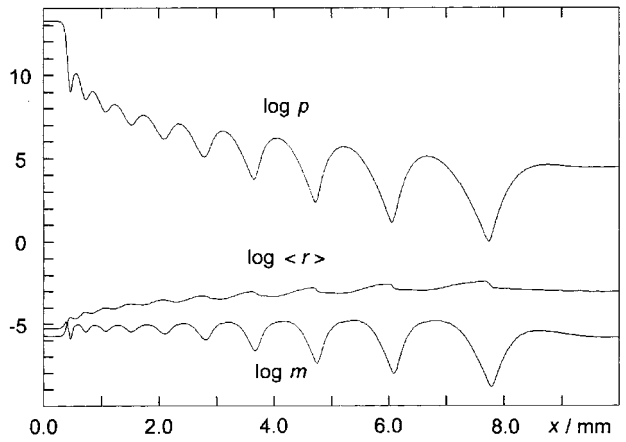

Figure 5. One-dimensional simulation of a Liesegang experiment according to the prenucleation system (2): Logarithmic plots of particle number density p (per cm^3), precipitate concentration m (in mol cm^{-3}), and average of particle radii $\langle r\rangle$ (in cm). Final state, after $t = 3{:}00$ h. A silver nitrate drop of $a_0 = 1.0$ M of 2 mm length placed on the left diffuses into a region with $b_0 = 5.14$ mM potassium chromate. Parameters are as given in the text, here with $w = 8.0 \times 10^{-8}$ cm.

Furthermore, the biggest particles are formed only between the precipitation maxima and not within them. The reason for this behavior is that at low values of supersaturation s the particles created with initial radii w or $w/\ln s$ can grow continuously over longer periods because s is not rapidly diminished by extensive particle creation. At the precipitation maxima, however, rapidly increasing supersaturation was immediately converted into a large number of small particles. After that conversion, the remaining supersaturation is too low to support continuous growth of the whole particle ensemble. Thus, the particles remain small at the maxima of the number density p.

Two-Dimensional Simulations. If diffusion of silver nitrate is supplied by an ideal circular or straight source, the results are concentric rings or parallel bands of precipitate. The interband distances are, in the case of strong electrolyte gradients, increasing with growing distance from the diffusion source and can be approximated by the well-known Jablczynski's law.[62]

Now let us consider the coupling of trains of precipitation bands emanated from nonideal diffusion sources. Figure 6 shows the simulated plot of two different trains of periodic precipitation evolved from a ragged silver nitrate source at the top of the area. Besides the edge of the diffusion source, parallel sets of bands have been formed with a distinct shift to one another caused by the source edge. Band shifts below half a local wavelength λ between adjacent sets are equalized by sigmoidal connections between the left and right bands. However, if the band shift attains half a wavelength, the former one-to-one connection of the bands is no longer maintained and the bands are connected by an apparent bifurcation or an anastomosis, in Liesegang's term. In other words, the system of connected bands behaves "elastically" as long as local displacements of half a wavelength are not attained (compare Figures 1−4). Figure 6 shows a series of such branch points because the relative displacements of the adjacent trains are about $\lambda/2$ in most of the area.

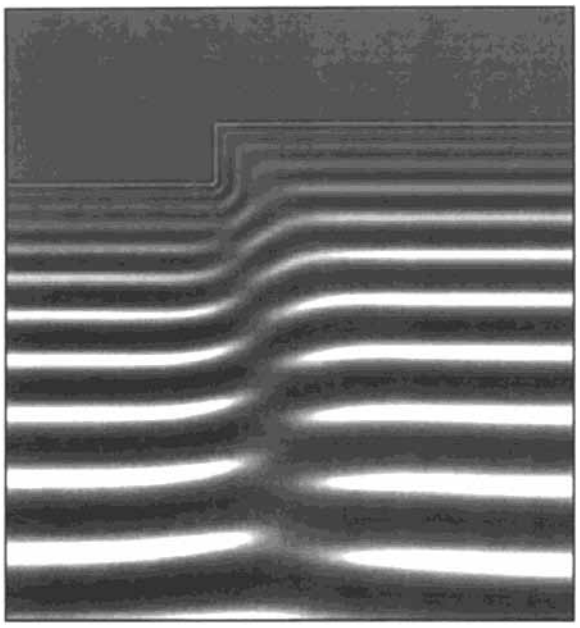

Figure 6. Two-dimensional simulation of a Liesegang experiment according to system (2). Final state, after 60 h. Grayplot of log m (precipitate concentrated m in mol cm^{-3}), grayscale in 255 steps between -8 (white) and -4 (black). Due to the ragged contour of the silver nitrate drop ahead, a series of branch points or anastomoses is created. Parameters follow Figure 5, here with $w = 1.0 \times 10^{-7}$ cm. Initial concentrations: $a_0 = 0.3$ M (contour ahead), $b_0 = 5.14$ mM. Horizontal field of view: 48 mm. Grid point density: 4 points per mm.

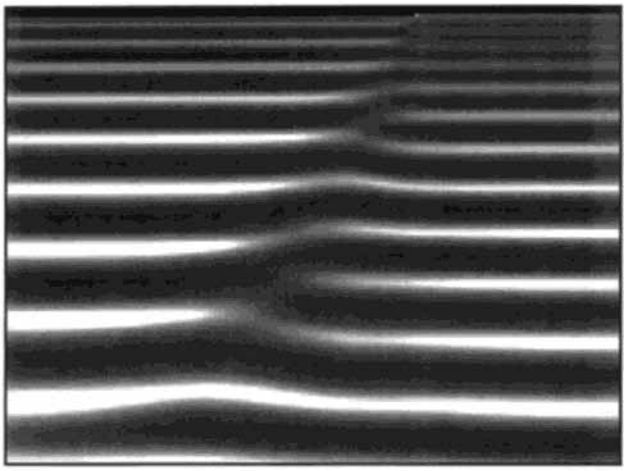

Figure 7. Two-dimensional simulation of a Liesegang experiment according to system (2). Final state, after 60 h. Grayplot of log m as in Figure 6. Here, diffusion of silver nitrate takes place across the open upper boundary with different source concentrations. Boundary concentrations: $a_0 = 0.1$ M on the left (0 to 34.5 mm) and $a_0 = 0.3$ M on the right (34.5 to 52 mm); $b_0 = 5.14$ mM. Horizontal field of view: 52 mm. Other parameters and scalings, see Figure 6.

The same result is obtained when a straight diffusion source involves a distinct concentration step as shown in Figure 7. The band trains have no initial band shift but develop with different spatial increments per band. The result is a increasing band shift between the left and the right train. The source concentration at the left side of the upper boundary in Figure 7 is one-third compared to the right part, thus the bands on the left evolve more widestanding than the right bands. The result is the formation of three anastomoses connecting both trains. Branch points can also be constructed if a ring system is built up by an unsymmetric polycentric diffusion source. In Figure 8, two centers with different silver nitrate concentrations force the

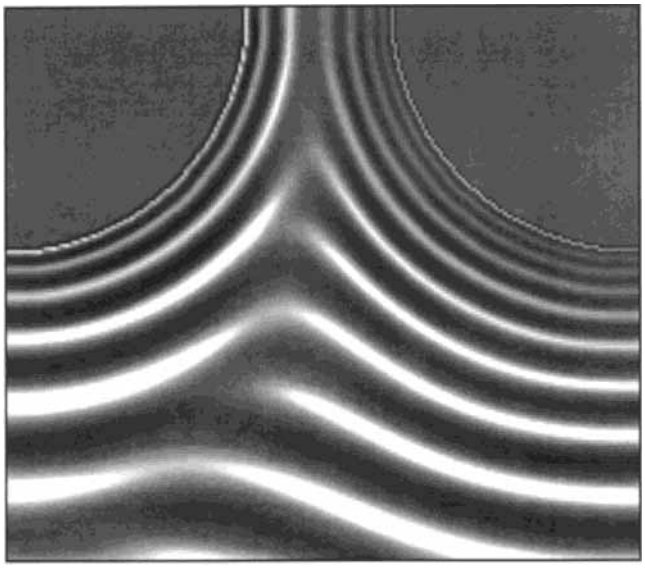

Figure 8. Two-dimensional simulation of a Liesegang experiment according to system (2). Final state, after 80 h. Grayplot of log m as in Figure 6. Here, diffusion of silver nitrate proceeds from a couple of drops ($r = 20$ mm) of different concentrations: $a_0 = 0.1$ M in the left and $a_0 = 0.3$ M in the right drop; $b_0 = 5.14$ mM. Horizontal field of view: 52 mm. Other parameters and scalings, see Figure 6.

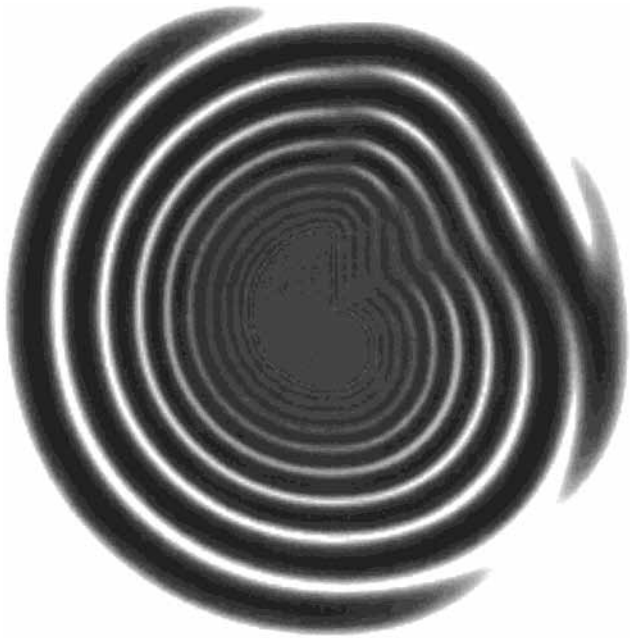

Figure 9. Simulation of a spiral system of Liesegang rings using system (2). Grayplot at $t = 83{:}20$ h. The radial symmetry breaking branch point is induced by the ragged contour of the central silver drop. Initial concentrations: $a_0 = 0.7$ M within the drop, $b_0 = 5.14$ mM throughout. Horizontal field of view: 74 mm (full simulation field: 88×88 mm). Other parameters and scalings, see Figure 6.

emanation of adjacent ring systems with individual wavelengths and, thus, apparent splitting of bands.

Figure 4 demonstrated how a branch point or anastomosis transforms a series of concentric rings into an outwardly winding spiral. An example of a simulated spiral is given in Figure 9. The upper right edge of the central diffusion source forces the creation of a branch point that prevents subsequent formation of closed rings, the resulting "free end" of banded precipitation forms a spiral. It should be noted here that, both in experiment and in numerical simulation, the spiral arms are not growing continuously in transversal directions. In fact, there appear at

first single filaments of precipitate which later join together, as also do concentric rings with nonideal symmetry. Figure 9 shows that the outer arm of the spiral is composed of filaments which will be joined later. Furthermore, the spiral arm exhibits on the right a second bifurcation that obviously will rearrange the concentrical symmetry of the ring system.

The formation of three-dimensional spirals[24,27,45,49−52] in cylindrical vessels mentioned above can in the same manner be considered a consequence of such symmetry breaking. Ideally, we observe in cylinders an ensemble of thin parallel disks. This translational symmetry can be broken by a little distortion at the junction between the outer and the inner electrolyte. This primary distortion may give rise to a sequence of precipitation disks with increasing undulations, until at one point the undulation jumps over to the beginning of a staircase winding downward.[52]

4. An Extended CPG Model

Let us now discuss a competitive particle growth (CPG) model which considers both formation of a colloidal turbidity zone prior to precipitation and Ostwald ripening, phenomena neglected in the model discussed above.

The CPG model after Ortoleva et al.[29−31,33] is based on the assumption of a constant and uniform particle number density n formed by a preceded nucleation process.[63] Competition of growing particles between related volume elements leads to formation of bands constituted of bigger particles separated by spaces of vanishing small particles at the expense of which the bigger within the bands have grown.

In our CPG model, we want to introduce the nucleation process explicitly with the formation of a colloid phase corresponding to the turbidity zone enclosing the outer precipitation ring. The colloid phase consists of very small particles of only a few molecules of silver chromate.[55] These conglomerates of molecules do not yet have a free surface like bigger particles to be treated energetically by the Gibbs−Thompson relation. Thus, such colloid phases may be stable at low values of supersaturation. Their stability is further supported by adsorption of gelatin particles thus acting as a protective colloid.[64]

Considering again the silver chromate reaction R1 from section 3, let the nucleation rate J of the colloid particles be

$$J(s) = k_j s^5 \tag{8}$$

Supersaturation $s = c/c_0$ is defined as above. Initial radii r_0 of the colloid particles are derived from a polynomial equilibrium function $s^{eq}(r)$ which comprises both colloid and developed solid particles (Figure 10). This polynomial function is defined as

$$s^{eq}(r) = 1 + \frac{w^3 r^3}{r^6 + r_c^6} \tag{9}$$

where w is the capillary length defined in eq 7. Here, $s^{eq}(r)$ attains its maximum at the critical value r_c separating the colloid phase ($r < r_c$) from the phase of solid particles ($r > r_c$), for which the Gibbs−Thompson relation $s^{eq}(r) = \exp(w/r)$ is approximated (Figure 10). Let the growth rate of the radii be

$$\frac{dr}{dt} = k_r c_0 [s - s^{eq}(r)] \tag{10}$$

The partial differential equations for our extended CPG system are identical to eq 2 from section 3. The main difference to the Dee system is the mass conversion term $dm/dt = u(x, t)$. After discretization of both space and time, the integral formulation of $m(x, t)$ in eq 3 can be transformed into a sum over an ensemble of distinct generations of growing (or decaying) particles once formed:

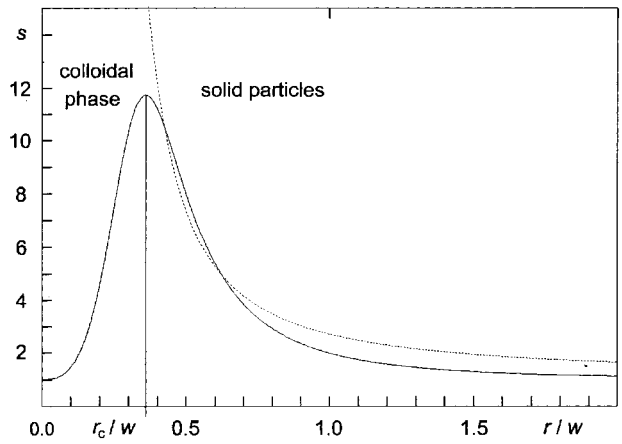

Figure 10. Equilibrium curves of supersaturation $s^{eq}(r)$ of the CPG system. Solid curve: polynomial function according to eq 9, with $r_c = 0.36\ w$. Dotted curve: Gibbs−Thompson relation $s^{eq}(r) = \exp(w/r)$.

$$m_{ij}(t) = \frac{4\pi}{3V_m} \sum_{k=1}^{n_G} p_{ijk} r_{ijk}^3(t) \tag{11}$$

V_m is the molecular volume of the precipitate, i and j are the indices of the discrete volume elements in vertical and horizontal direction, n_G is the particle generation number attained at time $t = t_0(i, j) + n_G \Delta t_G(i, j)$, and p_{ijk} is the local particle number density accumulated during the kth particle generation.

The particle ensembles are considered to be monodisperse within each generation. If supersaturation $s(i, j)$ exceeds any critical vale, say, $s_c = 1.1$, the first generation of colloid particles is created and grows (or later decays) according to eq 10. As long as $s > s_c$, further generations of durations $\Delta t_G(i, j)$ are created. With $s < s_c$, after the moving front of supersaturation has passed, the formation of new particles is terminated, but the growth or decay of the generations once formed is further considered. In our simulations, we limited the maximum number of generations in each volume element to $n_G^{max}(i, j) = 50$. Thus, the individual lengths of the generation time intervals $\Delta t_G(i, j)$ increase with the distance of the grid point (i, j) from the diffusion source of silver ions.

As long as $r < r_c$, particles created are considered as colloids and form a stable turbidity zone. When supersaturation s exceeds the maximum value $s_{max} = 1 + w^3/2r_c^3$ according to the equilibrium function (eq 9), the colloid particles attaining the radius r_c turn over to solid particles with thermodynamic behavior. Now they follow the Gibbs−Thompson relation and grow rapidly at the expense of local supersaturation and, consequently, at the expense of colloid phases in surrounding volume elements.

In our calculations, the value of capillary length was chosen to be $w = 1.45 \times 10^{-3}\ \mu$m. The values of the critical radius r_c were $0.36\ w$ and $0.45\ w$. Thus, the range of particle radii within the colloid phase in the model is far below the resolution limit of X-ray microscopy ($0.01\ \mu$m) employed in investigating the turbidity zone in experiment (section 2). A colloid particle with $r = 0.45w$ should, after a rough estimation, consists of about 11 molecules of silver chromate.

One-Dimensional Simulations. Figure 11 shows an example of a one-dimensional simulation of the extended CPG system.

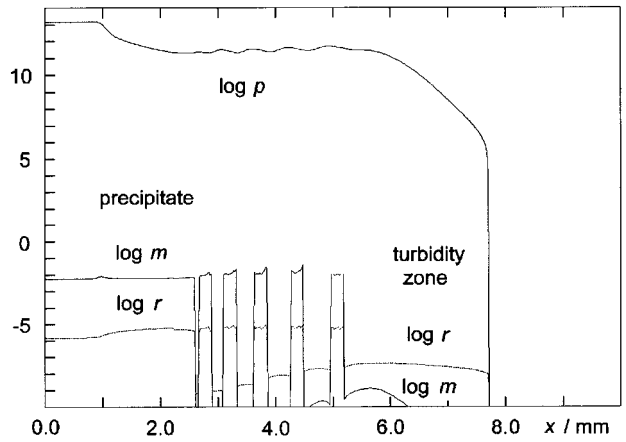

Figure 11. One-dimensional simulation of Liesegang bands with the extended CPG model. Plot at $t = 33{:}20$ min. Parameters $k_j = 1.0 \times 10^4$ cm^{-3} s^{-1}, $k_r = 1.0 \times 10^{-4}$ cm M^{-1} s^{-1}, $\sigma = 90.0$ erg cm^{-2} ($w = 1.45\ 10^{-7}$ cm), $r_c = 0.36\ w$. Concentrations: $a_0 = 1.0$ M between $x = 0$ and 1.0 mm; $b_0 = 5.14$ mM throughout; other parameters as in the Dee model (section 3). Particle number density p is scaled in cm^{-3}, solid mass density m in mol dm $^{-3}$, particle radius r (dotted) in cm.

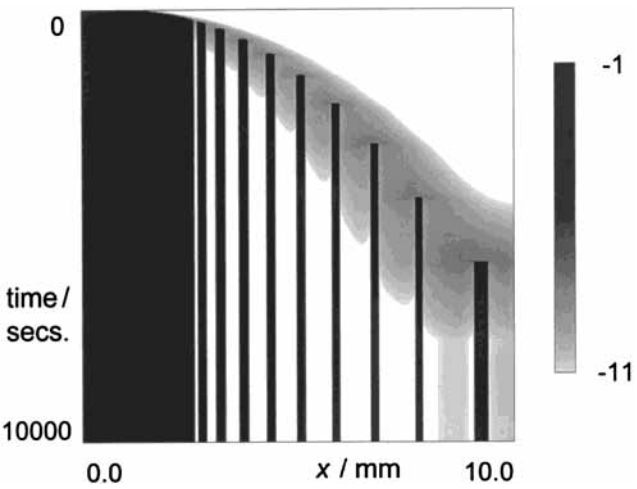

Figure 12. Grayplot of the spatiotemporal evolution of mass density log m after the extended CPG model. Parameters and scaling as in Figure 11.

The diffusion source from the left causes first a distinct zone of continuous precipitation which turns over to sharp bands with clear interband spaces. In front of the last precipitation band, a colloid zone with small particles is formed. This colloid phase is gradually consumed in the vicinities of the last and the preceding bands until these particles are completely removed between the bands. In contrast to the prenucleation model, the particle number density p is only weakly modulated here. The distinct periodicity of m in the CPG model is mainly due to the strong segregation of particles with different radii. The particle radii within the precipitation bands of Figure 11 attain values of about 0.1 μm, just 70 times greater than the capillary length w. These simulated radii coincide well with the particle radii of freshly precipitated rings (0.04 to 0.125 μm) obtained by in situ X-ray microscopy (section 2).

The grayplot of the same simulation (Figure 12) shows the continuous time evolution of such a sharp band system. It can clearly be seen, how dark bands are abruptly created from density maxima of the colloid zone and finally exhaust their feeding zones.

It should be noted that the phenomenon of Ostwald ripening, both in model and in experiment, works on two different time scales: Freshly arised ring particles are rapidly growing to the debit of the surrounding colloid particles. Only this process is pattern forming. At very larger time scales, competition between solid particles within the bands leads to a coarsening of the particle size distribution. This process is subsequent and not responsible for the formation of the bands themselves.

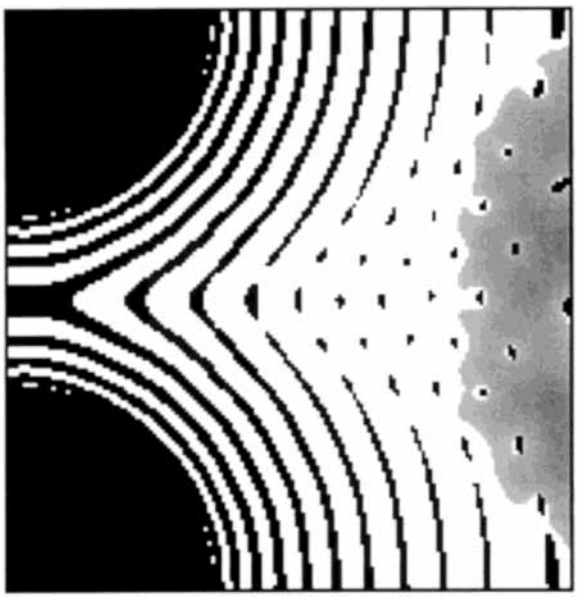

Figure 13. Two-dimensional simulation of a double-centered Liesegang system with the extended CPG model at $t = 6{:}00{:}00$ h. Grayplot of mass density log m showing dark bands of precipitate and a residual of the turbidity zone. Parameters: $k_j = 1.0 \times 10^5$ cm^{-3} s^{-1}, $k_r = 1.0 \times 10^{-5}$ cm M^{-1} s^{-1}, $r_c = 0.40\ w$. Concentrations: $a_0 = 1.0$ M within identical drops of $r = 3.5$ mm, $b_0 = 5.14$ mM throughout. Vertical field of view 16 mm, grid point density: 10 points per mm. Other parameters and scalings, see Figures 11 and 12.

Two-Dimensional Simulations. Numerical experiments with the extended CPG model show, besides the expected longitudinal periodicity of bands, also a transversal rhythm. This transversal periodicity may occur, if the mass density within the moving prenucleation front is transversally modulated by interference of different diffusion centers. Transition to solid phase occurs first at the maxima of the modulated front, thus giving rise to single precipitation filaments which remain isolated. Rapidly growing solid particles within single spots or filaments cause a draining of solute or colloidal material in both transversal directions.

Figure 13 shows a simulated Liesegang system generated by diffusion of silver ions from a couple of identical drops. The rings remain concentrical as long as the diffusion fields of each drop are undisturbed. After the third ring, both systems join to a lemniscate. This lemniscate is also found in the colloidal front whose density is slightly modulated with local maxima at the intersection points of undisturbed rings. Precipitation naturally starts at those local maxima and tries to continue in lateral directions. But with increasing distance from the diffusion sources, the diffusion halos of chromate ions B, and silver chromate C, respectively, become broader due to the shallower gradient of silver ions A. Local halos produced by the first filaments in the rings will not be equalized by diffusion as rapidly as in the first rings. Consequently, precipitation finally takes place only at the mentioned points of the intersection, thus forming a grid of filaments. The residual of the turbidity zone in the right part of Figure 13 shows clearly the draining effect of single spots in each direction. Such a double-periodic precipitation grid can be found in the right part of the Liesegang

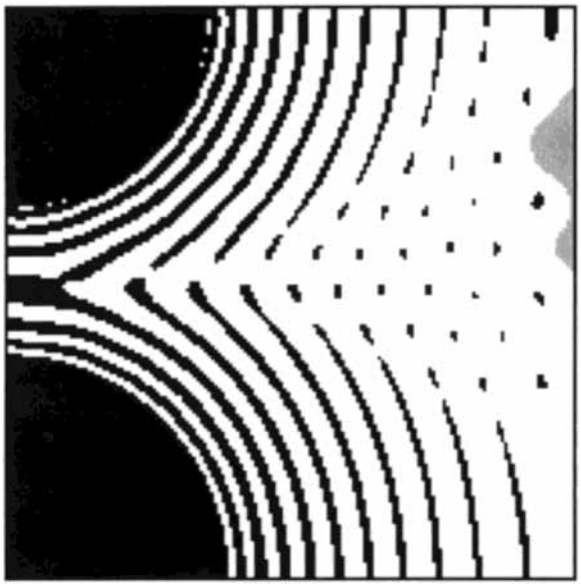

Figure 14. Two-dimensional simulation of a double-centered Liesegang system with the extended CPG model at $t = 6{:}50{:}00$ h. Grayplot of mass density log m. Initial concentrations: $a_0 = 1.5$ M (lower drop), $a_0 = 1.0$ M (upper drop). Radius of both drops: $r = 3.5$ mm, $b_0 = 5.14$ mM throughout. Other parameters and scalings, see Figure 13.

experiment in Figure 2. First observation of this double periodicity was made by Küster with lead iodide.[40]

If the concentration of the lower drop is increased, the result is the expected phase shift between the upper and the lower ring system (Figure 14). Phase differences are not equalized by sigmoidal bridges or anastomoses as obtained by the prenucleation model (Figure 8). Here, using the CPG model, phase differences induce a wedge of void space between the ring systems. The reason is the lower mass density of the colloidal front within the zone of adjacent ring systems compared to the rings themselves where precipitation starts first and leaves the central wedge blank. Also, the simulations with the prenucleation model in section 3 indicated that the mass density of the precipitate is slightly lower within the anastomoses than in the regular bands (Figures 6−8).

Figure 15 shows the development of bands from a diffusion source with sigmoidal contour. The contour generates independent band systems which are separated by a central wedge bearing a tall stripe of bands with shifted phase (compare Figure 2). A second wedge rises near the right bottom of the picture. The same idea of forced phase shift is accomplished in Figure 16. Autonomous band systems are here created by different silver ion concentrations at the straight upper boundary. The result is a clear wedge that opens after the phase difference between the trains has achieved the value of about $\lambda/2$.

5. Discussion

Liesegang rings, even when constricted to precipitation of silver chromate, appear in manifold fashions depending on the nature of the diffusion medium. In silica gel, only chains of single crystals are formed instead of continuous rings of amorphous precipitate.[37] Continuous rings both with branch points and blank alleys are obtained in gelatin gels (Figures 1−4). Gelatin is known to serve both as protective colloid, stabilizing the colloid phase, and poisoning colloid,[64] which hinders freshly formed particles from rapid and radius-dependent growth at the expense of solute phase. Thus, Ostwald ripening leading to coarsening to a few single crystals of silver chromate does not take place in gelatin systems.

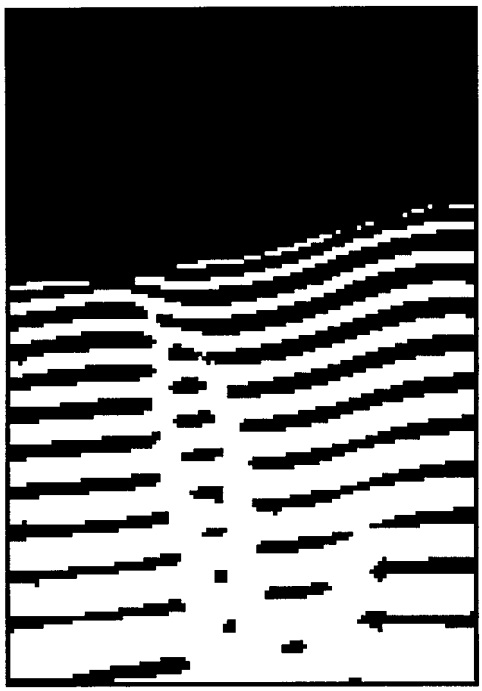

Figure 15. Two-dimensional simulation of a Liesegang system with the extended CPG model. Final state, at $t = 6{:}50{:}00$ h. Grayplot of mass density log m. Initial concentrations: $a_0 = 1.0$ M within a sigmoidal contour at the top of the field, $b_0 = 5.14$ mM throughout, $r_c = 0.45\ w$. Other parameters and scalings, see Figure 13. Horizontal field of view: 11.2 mm.

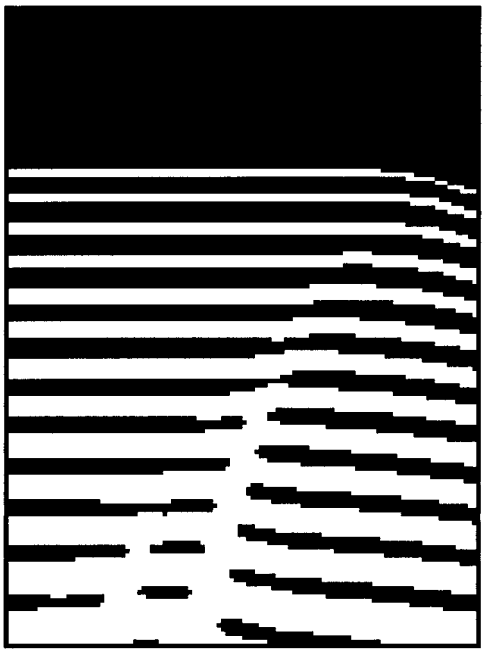

Figure 16. Two-dimensional simulation of a Liesegang system with the extended CPG model. Final state, at $t = 6{:}50{:}00$ h. Grayplot of mass density log m. Here, silver nitrate with different concentrations: $a = 1.0$ M at the left (0 to 12.2 mm) and $a = 3.0$ M at the right (12.2 to 14.4 mm) part intruded from the upper boundary, $b_0 = 5.14$ mM throughout, $r_c = 0.45\ w$. Other parameters and scalings, see Figure 13. Horizontal field of view of the left cut seen here: 11.2 mm, (14.4 mm of the full picture).

The prenucleation model (section 3) is rather appropriate for systems with inhibited particle growth. Commonly observed pattern characteristics such as branch points and spiralizations can comfortably be simulated with the prenucleation model where the particle growth is not radius dependent. On

the other hand, the prenucleation model does not describe the formation of a turbidity zone of embryonic nuclei from which the rings finally arise. Clear spaces between the rings can only enforced by special assumptions on the nucleation rate. But assumption of vanishing nucleation rate at low supersaturations[21] contradicts the occurrence of a continuous, nonperiodic colloidal front prior to the ring systems.

The extended CPG model (section 4) comprises both formation of a turbidity zone at lower supersaturations and, after a certain critical radius r_c is exceeded, a subsequent growth of solid particles at the expense of the colloidal zone. The results of this model are sharp bands, void spaces between the bands, and morphological defects of the bands (alleys of gaps and transversal rhythm of filaments). Branch points of continuous rings found with the prenucleation system are replaced by void gaps because of the strong competition of growing particles with the colloidal phase. Appropriate modification on the equilibrium function s^{eq} (eq 9) such as the introduction of a certain particle radius limit should simulate the poisoning effect of gelatin on the surfaces of growing particles, thus delivering more continuous bands with branch points or anastomoses.

Acknowledgment. We are indebted to Dr. J. Thieme (Göttingen) for in situ X-ray microscopic measurements on Liesegang systems and Dr. L. Pohlmann (Berlin) for helpful discussions on the prenucleation model.

References and Notes

(1) Ord, W. M. *On the Influence of Colloids upon Crystalline Form and Cohesion*; E. Stanford: London, 1879.

(2) Liesegang, R. Ed. Chemische Fernwirkung. *Lieseg. photograph. Arch.* **1896**, *37* (800), 305−309, continued in (801), 331−336. A-Linien *Lieseg. photograph. Arch.* **1896**, *37* (801), 321−326. Über einige Eigenschaften von Gallerten *Naturwiss. Wochenschr.* **1896**, *11*, 353. The genesis of his early works on ring formation is described in Liesegang's autobiography "Und doch!" in: Krug, H.-J.; Pohlmann, L., Eds. *Evolution und Irreversibilität*; Duncker & Humblot: Berlin, 1997; pp 215−296.

(3) Liesegang, R. Ed. *Geologische Diffusionen*; Th. Steinkopf: Dresden and Leipzig, 1913.

(4) Liesegang, R. Ed. *Die Achate*; Th. Steinkopf: Dresden and Leipzig, 1915.

(5) Ortoleva, P. *Geochemical Self-Organization*; Oxford University Press: Oxford, New York, 1994.

(6) Leduc, S. *Das Leben in seinem physikalisch-chemischen Zusammenhang*; L. Hofstetter: Halle, 1912.

(7) Küster, E. *Über Zonenbildung in kolloidalen Medien*; G. Fischer: Jena, 1913, 1931.

(8) Hedges, E. S.; Myers, J. E. *The Problem of Physicochemical Periodicity*; Longmans Green: London, 1926.

(9) Hedges, E. S. *Liesegang Rings and Other Periodic Structures*; Chapman and Hall: London, 1932.

(10) Henisch, H. K. *Crystals in Gels and Liesegang Rings*; Cambridge University Press: Cambridge, 1988.

(11) Henisch, H. K. *Periodic Precipitation*; Pergamon Press: Oxford, 1991.

(12) Stern, K. H. *Bibliography of Liesegang Rings*, 2nd ed.; U.S. Government Printing Office: Washington D.C., 1967.

(13) Kuhnert, L.; Niedersen, U. *Selbstorganisation chemischer Strukturen. = Ostwalds Klassiker der exakten Wissenschaften*, Geest & Portig: Leipzig, 1987; Vol. 272.

(14) Spotz, E. L.; Hirschfelder, J. O. Liesegang ring formation arising from diffusion of ammonia and hydrogen chlorine gases through air. *J. Chem. Phys.* **1951**, *19*, 1215.

(15) Senf, L. Rhythmic precipitation (Liesegang rings) in gases. *Z. Phys. Chem. (Leipzig)* **1989**, *270*, 1020−1022.

(16) Flicker, M.; Ross, J. Mechanism of chemical instability for periodic precipitation. *J. Chem. Phys.* **1974**, *60*, 3458−3456.

(17) McBirney, A. R.; Noyes, R. M. Crystallization and layering of the Skaergaard intrusion. *J. Petrol.* **1973**, *20*, 487−554.

(18) Ostwald, W.; A-Linien von R. E. Liesegang (review) *Z. Phys. Chem. (Leipzig)* **1897**, *23*, 356; *Lehrbuch der allgemeinen Chemie*, 2. Aufl., II, 2.: *Verwandtschaftslehre*; Engelmann: Leipzig, 1899; p 779.

(19) Prager, S. Periodic precipitation *J. Chem. Phys.* **1956**, *25*, 279−283.

(20) Dee, J. T. Patterns produced by precipitation at a moving reaction front. *Phys. Rev. Lett.* **1986**, *57*, 275−278; The patterns produced at a moving reaction front. *Physica D* **1986**, *23*, 340−344.

(21) Le Van, M. E.; Ross, J. Measurements and a hypothesis on periodic precipitation processes. *J. Phys. Chem.* **1987**, *91*, 6300−6308.

(22) Dhar, N. R.; Chatterji, A. C. Theorien der Liesegangringbildung, *Kolloid.-Z.* **1925**, *37*, 2−9, 89−97.

(23) Büki, A.; Kárpáti-Smidróczki, E.; Zrínyi, M. Experimental and theoretial investigation of static and dynamic chemical pattern formations in gels. *Prog. Colloid. Polym. Sci.* **1996**, *102*, 110−117.

(24) Ostwald, Wo. Zur Theorie der Liesegang'schen Ringe. *Kolloid-Z.* **1925**, (Suppl. to Vol. 36, R. Zsigmondy Festschrift), 380−390.

(25) Chopard, B.; Luthi, P.; Droz, M. Reaction−diffusion cellular automaton model for the formation of Liesegang patterns. *Phys. Rev. Lett.* **1994**, *72*, 1384−1387.

(26) Feinn, D.; Ortoleva, P.; Scalf, W.; Schmidt, S.; Wolff, M. Spontaneous pattern formation in precipitating systems. *J. Chem. Phys.* **1978**, *69*, 27−39.

(27) Müller, S. C.; Venzl, G. Pattern formation in precipitation processes. In Modelling of Patterns in Space and Time, *Lecture Notes Biomath.*; Jäger, W., Murray, J. D., Eds.; Springer: Berlin, Heidelberg, New York, Tokyo, 1984; Vol. 55, pp 254−278.

(28) Kai, Sh. Gradient-free structures in Liesegang phenomena. In Spatio-Temporal Patterns in Nonequilibrium Complex Systems; Cladis, P. E., Palffy-Muhoray, P., Eds.; Nato Adv. Res. Workshop 1993; Addison-Wesley: Reading, MA, 1995; pp 445−468.

(29) Ortoleva, P. Solute reaction mediated precipitate patterns in cross gradient free systems. *Z. Phys. B: Condens. Matter*, **1982**, *49*, 149−156.

(30) Feeney, R.; Schmidt, S. L.; Strickholm, P.; Chadam, J.; Ortoleva, P. Periodic precipitation and coarsening waves: Applications of the competitive particle growth model. *J. Chem. Phys.* **1983**, *78*, 1293−1311.

(31) Sultan, R.; Ortoleva, P. Periodic and aperiodic macroscopic patterning in two precipitate post-nucleation systems. *Physica D* **1993**, *63*, 202−212.

(32) Lifshitz, I. M.; Slyozov, V. V. The kinetics of precipitation from supersaturated solutions. *J. Phys. Chem. Solids* **1961**, *19*, 35−50.

(33) Ortoleva, P. From nonlinear waves to spiral and speckle patterns. *Physica D* **1984**, *12*, 305−320.

(34) Krug, H.-J.; Jacob, K. H. Genese und Fragmentierung rhythmischer Bänderungen durch Selbstorganisation. *Z. Dtsch. Geol. Ges.* **1993**, *144*, 451−460.

(35) Krug, H.-J.; Jacob, K. H.; Dietrich, S. The formation and fragmentation of periodic bands through precipitation and Ostwald ripening. In Kruhl, J. H., Ed.; *Fractals and Dynamic Systems in Geoscience*; Springer: Berlin, Heidelberg, New York, 1994; pp 269−282.

(36) Polezhaev, A. A.; Müller, S. C. Complexity of precipitation patterns: Comparison of simulation with experiment. *Chaos* **1994**, *4*, 631−636.

(37) Krug, H.-J.; Brandtstädter, H.; Jacob, K. H. Morphological instabilities in pattern formation by precipitation and crystallization processes. *Geol. Rundsch.* **1996**, *85*, 19−28.

(38) Liesegang, R. Ed. Zur Übersättigungstheorie einiger scheinbar rhythmischer Reaktionen. *Z. Phys. Chem. (Leipzig)* **1911**, *75*, 371−373.

(39) Liesegang, R. Ed. Über die Reifung von Silberhalogenidemulsionen. *Z. Phys. Chem. (Leipzig)* **1911**, *75*, 374−377.

(40) Küster, E. Über die morphologischen Charaktere der Liesegang'schen Ringe. *Kolloid-Z.* **1916**, *18*, 107−116.

(41) Liesegang, R. Ed. Silberchromatringe und -spiralen. *Z. Phys. Chem. (Leipzig)* **1914**, *88*, 1−12.

(42) Liesegang, R. Ed. Pseudoklase. *Neues Jahrb. für Min. Geol. Pal.* **1914**, *39* (Suppl. Vol., Max Bauer Festschrift), 268−276.

(43) Kuo, Ch. Sh.; López Cabarcos, E.; Bansil, R. Two-dimensional pattern formation in reaction−diffusion systems. Influence of the geometry. *Physica A* **1997**, *239*, 120−128.

(44) Büki, A.; Kárpáti-Smidróczki, E.; Zrínyi, M. Two-dimansional chemical pattern formation in gels. Experiments and computer simulation. *Physica A* **1995**, *220*, 357−375.

(45) Kárpáti-Smidróczki, E.; Büki, A.; Zrínyi, M. Pattern-forming precipitation in gels due to coupling of chemical reactions with diffusion. *Colloid. Polym. Sci.* **1995**, *273*, 857−565.

(46) Rothmund, V. *Löslichkeit und Löslichkeitsbeeinflussung. = Handbuch der Angewandten Physikalischen Chemie in Einzeldarstellungen*. (Hrsg. G. Bredig) Vol. 7, Joh. Ambr. Barth: Leipzig 1907; pp 5−14.

(47) Liesegang, R. Ed. *Chemische Reaktionen in Gallerten*; Th. Steinkopff: Leipzig, 1924; p 67.

(48) Liesegang, R. Ed. Spiralenbildung bei Niederschlägen in Gallerten. *Kolloid-Z.* **1939**, *87*, 57−58.

(49) Tillmans, J.; Heublein, O. Neues von den Liesegangschen Ringen. *Umschau (Frankfurt a. M.)* **1914**, *19*, 930−933.

(50) Hatschek, E. Der Einfluss des Lichtes auf Bleichromat-Schichtungen. *Kolloid-Z.* **1925**, *37*, 297−298.

(51) Müller, S. C.; Kai, S.; Ross, J. Curiosities in periodic precipitation patterns. *Science* **1982**, *216*, 635−637.

(52) Chernavskii, D. S.; Polezhaev, A. A.; Müller, S. C. A model of pattern formation by precipitation. *Physica D* **1991**, *54*, 160−170.

(53) Hatschek, E. Silberchromatschichtungen in Kieselsäuregel. *Kolloid-Z.* **1926**, *38*, 151−154.

(54) Kai, S.; Müller, S. C.; Ross, J. Measurements of temporal and spatial sequences of events in periodic precipitation processes. *J. Chem. Phys.* **1982**, *76*, 1392−1406.

(55) Lexa, D.; Holba, V. Periodic precipitation of silver chromate/dichromate in gelatin. *Colloid Polym. Sci.* **1993**, *271*, 884−890.

(56) Venzl, G.; Ross, J. Nucleation and colloidal growth in concentration gradients (Liesegang rings). *J. Chem. Phys.* **1982**, *77*, 1302−1307.

(57) Büki, A.; Kárpáti-Smidróczki, E.; Zrínyi, M. Computer simulation of regular Liesegang structures. *J. Chem. Phys.* **1995**, *103*, 10387−10392.

(58) López Cabarcos, E.; Kuo, Ch. Sh.; Scala, A.; Bansil, R. Crossover between spatially confined precipitation and periodic pattern formation in reaction diffusion systems. *Phys. Rev. Lett.* **1996**, *77*, 2834−2837.

(59) Kuo, Ch. Sh.; López Cabarcos, E.; Scala, A.; Bansil, R. Kinetics of spatially confined precipitation and periodic pattern formation. *Physica A* **1997**, *239*, 390−403.

(60) *Gmelin. Handbuch der anorganischen Chemie. Silber. Teil B 4*; Springer: Berlin, Heidelberg, New York, 1974; pp 294, 297, 301.

(61) We assume that the value $\sigma = 575$ erg cm^{-2} for silver chromate estimated from dissolution of big crystals between 0.3 and 50 μm (see ref 60) may not be applicable to the embryonic particles created prior to Liesegang rings and should be replaced by a much lower value. Therefore, we used $\sigma = 90$ erg cm^{-2} in section 4.

(62) Jablczynski, K. *Bull. Soc. Chim.* **1923**, *33*, 1592.

(63) This is a valid assumption for heterogeneous precipitation in grained media where n is identical with the particle number density of the grains. See: Sultan, R.; Ortoleva, P.; De Pasquale, F.; Tartaglia, P. Bifurcation of the Ostwald−Liesegang supersaturation−nucleation−depletion cycle. *Earth-Sci. Rev.* **1990**, *29*, 163−173.

(64) Zsigmondy, R. *Kolloidchemie*, 3. Aufl.; Otto Spamer: Leipzig, 1920; p 95.